Kovove Mater. 59 2021 303–313
DOI: 10.4149/km_2021_5_303

Study on the mechanical properties, wear resistance and microstructure of nano-SiC_p/ZA38 composite material under the synergistic effects of thermal-force-acoustic field

S. Liu[1], Y. Sima[1], L. Zhang[1], J. Zhang[1], W. Qiao[2], Q. Yuan[1,3]*

[1] *The State Key Laboratory of Refractories and Metallurgy, Key Laboratory for Ferrous Metallurgy and Resources Utilization of Ministry of Education, Wuhan University of Science and Technology, Wuhan 430081, P. R. China*
[2] *Wuhan Heavy Industry Casting & Forging Co. LTD., China State Shipbuilding Corporation Limited, Wuhan 430080, P. R. China*
[3] *Jiangsu Huaneng Cable Company Limited, Gaoyou 225613, Jiangsu, P. R. China*

Received 17 March 2021, received in revised form 21 May 2021, accepted 6 October 2021

Abstract

The nano-SiC_p/ZA38 composites reinforced by nano SiC particles were fabricated by stirring assisted ultrasonic vibration. To establish the influence of the fusant temperature, stirring speed, and ultrasonic power on the mechanical and tribological properties of the cast nano-SiC_p/ZA38 composite material, orthogonal experiments in four different fusant temperatures, stirring speed, and ultrasonic power were conducted. The synergistic effects of the thermal-force-acoustic field aroused by melting, stirring, and ultrasonic vibration were investigated. It was observed that the wear rate decreased with the dimension of the primary dendrite arm spacing. The wear rate of fabricated composite material decreased to a minimum value of 0.0042 mm s^{-1} when melting at 730 ℃, stirring with a speed of 300 rpm and ultrasonic vibration with a power of 850 W. The hardness reached 163.9 HV, and the compression strength reached 803 MPa. It was concluded that the acoustic field works prominently in improving the mechanical properties of the nano-SiC_p/ZA38 composite, while the thermal and acoustic fields play a major part in the friction and wear properties. Thus, the force field gets converted into an assistant field. In addition, the simultaneously or solely increased thermal-force-acoustic field does not ensure a considerable enhancement in the mechanical and tribological properties of the nano-SiC_p/ZA38 composite.

K e y w o r d s: composite, ultrasonic vibration, tribological property, microstructure, orthogonal experiment, acoustic field

1. Introduction

Aluminum (Al)-zinc (Zn)-based alloys have found their use in various machine components, especially in the area of mechanical transmission such as in bearing bush, bearing, slider, and piston due to their outstanding characteristics [1, 2]. Al-Zn-based alloys with a high percentage of metals have a low melting point, special casting property, good machinability, excellent wear and corrosion resistance at room temperature, and high strength. Besides, the low cost for producing the aforementioned mechanical transmission components makes the high Al-Zn-based alloy welcomed. However, a decrease in mechanical properties caused by increasing temperature due to friction makes some high Al-Zn-based alloys used in the high speed and heavy load conditions invalid. To improve the mechanical properties at high friction temperature of the Al-Zn-based alloys, some nano SiC particles with stable thermophysical properties are often added in these Al-Zn-based alloys to produce the metal matrix composites reinforced by ceramics. The metal matrix composites reinforced by ceramics have come into the limelight in recent years owing to their superior physical, mechanical, electrochemical, and frictional wear properties [3, 4]. There are many methods to fabricate the

*Corresponding author: e-mail address: yuanqing@wust.edu.cn

metal matrix composites reinforced by ceramics. The key issue to improve the mechanical properties is to effectively control the homogeneous distribution of the reinforced particles in the metal matrix [5–8]. The stir casting technique is a relatively easy technique for industrialization. However, the process defects, such as the macroscopic as-cast structure and the composition cluster, demand prompt solutions. The reinforced particles react with the interface of the metal matrix, resulting in shrinkage related porosity [2, 9].

Literature studies show that stirring assisted ultrasonic vibration employed to fabricate the composite is effective in refining and balancing the casting microstructure [10–14]. Khosravi et al. have reported the effects of stirring temperature and speed on the distribution of the reinforced particles in the metal matrix. The mechanical properties of the A356-SiC_p composites were also discussed in detail. However, the effects of ultrasonic vibration on the microstructure and properties of the composites were not mentioned [15]. Wang et al. fabricated the micro-SiC particle reinforced magnesium matrix composites, having a varied composition of reinforced particles by the stir casting assisted by ultrasonic treatment. In their research, the processing, microstructure, and mechanical properties of the composites were fully analyzed. The results demonstrated that ultrasonic treatment significantly improved stir casting and mechanical properties. However, less information on the effects of fabricating processes such as the fusant temperature, stirring speed, and ultrasonic power on the microstructure and mechanical properties of composites has been provided [16]. K. Hu et al. [17] and A. H. Idrisi et al. [18] reported that ultrasonic treatment substantially improved the mechanical properties of composites. The analysis of the fusant temperature, stirring speed, and thermal-force-acoustic field due to the stir casting assisted ultrasonic vibration was insufficient.

It is well known that the thermal field of the fusant formed during melting, the force field generated by the stirring, and the acoustic field aroused by the ultrasonic vibration are concomitant in the stir casting assisted by ultrasonic treatment processing. The synergistic effect of the thermal-force-acoustic field plays a vital role in improving the mechanical properties of composites. However, in most studies, only one or two fields were analyzed. To further investigate the relationships between the thermal-force-acoustic fields on the microstructure and mechanical properties of metal matrix composites reinforced by ceramics, it is necessary to conduct vast theoretical experiments. The multiple factors involved in the stir casting assisted by ultrasonic treatment processing necessitate various time-consuming experiments. The orthogonal experiment is often used to determine the effect of the single factors [19–25]. In this study, orthogonal experiments were used to identify the relationships among the fusant temperature, stirring speed, and ultrasonic power on the mechanical and tribological properties of cast nano-SiC_p/ZA38 composite material reinforced by nano SiC particles. Four different fusant temperatures, stirring speeds, and ultrasonic powers were considered for the experiments. The results in the present investigation will guide the fabrication process of nano-SiC_p/ZA38 composite material reinforced by nano SiC particles.

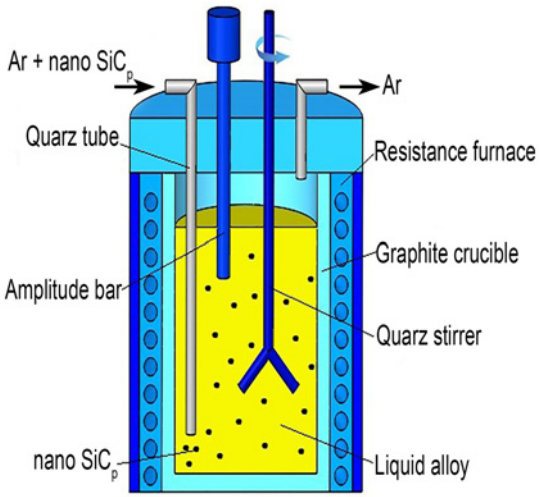

Fig. 1. The schematic diagram for the fabrication of nano-SiC_p/ZA38 composite.

2. Materials and methods

2.1. Composite fabrication

The nano-SiC_p/ZA38 composite fabrication was done using zinc ingot (0#), 99.99 wt.% Al ingot, H68 Cu-Zn alloy, 99.99 wt.% magnesium (Mg) particles, and SiC nanoparticles with a dimension of 80 nm as raw materials. The addition amount of nano SiC particles was 0.3 wt.%, and the actual composition of the composite was 38Al-2.5Cu-0.8Mg-0.3SiC--Zn (bal.). The schematic diagram for the fabrication of nano-SiC_p/ZA38 composite is presented in Fig. 1. The prepared Al ingot was put in the graphite crucible and then placed in the resistance furnace to be heated till it melted. The zinc ingot, H68 Cu-Zn alloy, and Mg particles were sequentially added in the melting Al fusant. After isothermal holding, the temperature of the graphite crucible was adjusted to the pre-set values. The SiC nanoparticles were added by the high-pressure jetting powder process by introducing Argon (Ar) gas. The usage of Ar avoids unnecessary oxidation. The stirring process and ultrasonic vibration were simultaneously conducted under the protection of Ar. Table 1 presents the designed

Table 1. Designed thermal-force-acoustic fields with different fusant temperatures, mechanical stirring speeds and ultrasonic power during the smelting

Fusant temperature (℃)	Mechanical stirring speed (rpm)	Ultrasonic power (W)
700	100	300
730	200	450
760	300	600
800	400	850

Table 2. Mechanical and tribological properties of specimens fabricated by orthogonal experiments

Specimen	Thermal-force-acoustic field			Wear rate ($mm\,s^{-1}$)	Hardness HV	Compressive strength (MPa)
	Temperature (℃)	Stirring speed (rpm)	Ultrasonic power (W)			
1	700	100	300	$0.0279^{+0.0002}_{-0.0005}$	$142.9^{+0.2}_{-0.15}$	635^{+5}_{-4}
2	700	200	450	$0.0206^{+0.0003}_{-0.0004}$	$145.4^{+0.2}_{-0.1}$	655^{+3}_{-2}
3	700	300	600	$0.0197^{+0.0002}_{-0.0003}$	$146.2^{+0.1}_{-0.15}$	670^{+5}_{-2}
4	700	400	850	$0.0085^{+0.0005}_{-0.0005}$	$158.5^{+0.1}_{-0.1}$	782^{+4}_{-3}
5	730	100	450	$0.0165^{+0.0004}_{-0.0002}$	$147.7^{+0.2}_{-0.2}$	674^{+5}_{-6}
6	730	200	300	$0.0103^{+0.0005}_{-0.0004}$	$151.6^{+0.15}_{-0.15}$	736^{+4}_{-6}
7	730	300	850	$0.0042^{+0.0003}_{-0.0006}$	$163.9^{+0.1}_{-0.15}$	803^{+3}_{-4}
8	730	400	600	$0.0095^{+0.0004}_{-0.0005}$	$155.5^{+0.2}_{-0.1}$	752^{+5}_{-6}
9	760	100	600	$0.0098^{+0.0005}_{-0.0006}$	$153.2^{+0.1}_{-0.1}$	750^{+2}_{-3}
10	760	200	850	$0.0073^{+0.0002}_{-0.0002}$	$163.2^{+0.15}_{-0.15}$	798^{+6}_{-3}
11	760	300	300	$0.0132^{+0.0004}_{-0.0005}$	$151.1^{+0.2}_{-0.15}$	714^{+7}_{-5}
12	760	400	450	$0.0078^{+0.0003}_{-0.0004}$	$162.5^{+0.1}_{-0.15}$	786^{+4}_{-7}
13	800	100	850	$0.0098^{+0.0002}_{-0.0003}$	$152.9^{+0.2}_{-0.1}$	746^{+5}_{-8}
14	800	200	600	$0.0088^{+0.0003}_{-0.0004}$	$163.2^{+0.1}_{-0.1}$	786^{+9}_{-4}
15	800	300	450	$0.0158^{+0.0004}_{-0.0005}$	$150.4^{+0.2}_{-0.15}$	685^{+6}_{-8}
16	800	400	300	$0.0179^{+0.0005}_{-0.0005}$	$146.4^{+0.2}_{-0.15}$	671^{+7}_{-4}

thermal-force-acoustic fields containing different fusant temperatures, mechanical stirring speed, and ultrasonic power during smelting. The total action time for the thermal-force-acoustic field was about 5 min. After 2 min standing of the final composite melting, slagging-off and casting process were consecutively carried out. In the end, the preparation of the as-cast nano-SiC_p/ZA38 composite reinforced by nano SiC was successful.

2.2. Material characterization

Room temperature compression tests were carried out on a WE-100 hydraulic universal material testing machine. Before the compression process, the two contact surfaces of the specimens were both polished by a 1500 grade abrasive paper to remove the surface scratch and ensure parallel between each side of the specimen. Graphite wafers with a thickness of 0.1 mm were placed on the contact surfaces of the specimens. The displacement loading speed of the squeeze head was set at 1 mm min^{-1}. Micro-hardness tests were conducted on an HV-1000 micro-hardness tester with a loading force of 1.961 N. Duplicated hardness tests were carried out for each specimen. Cylindrical specimens with a dimension of ø 8 mm × 30 mm were machined to perform the dry-friction wear test on a frictional wear testing machine. The abrasive disc was made of GCr15 bearing steel. The degree of surface roughness (*Ra*) was calculated to be 6.3. The frictional pressure, friction velocity, and time values were determined to be 1.2 MPa, 840 rpm, and 10 min, respectively. The frictional wear rate was calculated by the length loss per unit distance, and the derivative of wear rate was considered the wear resistance coefficient.

Metallographic specimens were prepared for observing the as-cast microstructure and fracture morphology of specimens treated by different processing parameters. Related metallographic preparation methods have been previously described [26–30]. A ZEISS optical microscope (OM) and a field-emission scanning electron microscope (FE-SEM) with an energy dispersive spectroscopy (EDS) were used for the studies. Point analysis was done to determine the composition of the SiC particles. X-ray diffraction (XRD)

was used to detect the different phases in the fabricated composites.

3 Results and discussion

3.1. Mechanical and tribological properties

Table 2 shows the mechanical and tribological properties of different specimens fabricated by orthogonal experiments. The data indicate considerable differences in the micro-hardness, the compression strength, and the wear rate values of the specimens fabricated by different thermal-force-acoustic fields. Specimen 7 melted at 730 ℃, stirred at a speed of 300 rpm, and ultrasonically treated with a power of 850 W has the most commendable properties among all specimens. The wear rate of specimen 7 was 0.0042 mm s^{-1}, the smallest recorded among all other specimens under study. The hardness (163.9 HV) and the compression strength (803 MPa) were found to be the maximum.

Figure 2 shows the variance analyses of the mechanical and tribological properties affected by the fusant temperature, mechanical stirring speed, and ultrasonic power. Quadratic sum and mean square deviation in each parameter have been calculated. Fusant temperature and ultrasonic power greatly affected the wear rate compared to the stirring speed. The thermal and acoustic fields play a vital role in improving the wear resistance of the nano-SiC_p/ZA38 composite. The thermal and acoustic fields have a similar effect on the wear rate. The effect of acoustic field (ultrasonic power) is the maximum in the case of microhardness and compression strength compared to the effects of thermal and force fields. The force field was found to have a minimum influence in this regard. In short, the acoustic field has a greater effect than the thermal and force fields in enhancing the properties of the nano-SiC_p/ZA38 composite. The thermal and acoustic fields play a major part in the friction and wear properties of the specimens, where the force field serves as a supplementary field.

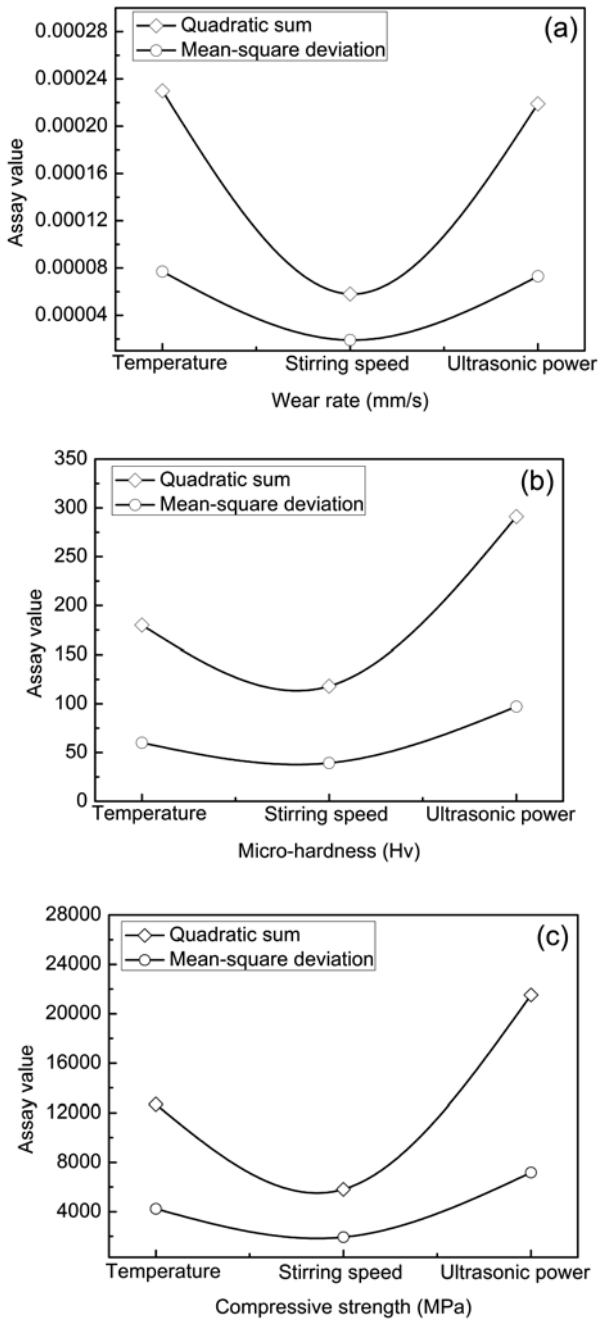

Fig. 2. Variance analyses for the mechanical and tribological properties.

3.2. Microstructure

According to the results in Table 2 and Fig. 2, a rational screening process was made. Five representative as-cast microstructures treated by different thermal-force-acoustic fields corresponding to the specimens 2, 6, 7, 10, and 15 are shown in Fig. 3. The as-cast microstructures of the various specimens are different from each other. The grain dimension in specimen 7 is uniform and refined compared to that of the other specimens. Moreover, the amount of dendritic crystal in specimen 7 is the least. X-ray diffraction and point analysis were carried out to determine the phases of the composite. Figure 4 shows the XRD and EDS results of specimen 7. It reveals that the main phase of the composite is the Al-Zn solid solution (Al, Zn). Furthermore, the composite contains the Al-rich α(Al, Zn) phase (Fig. 4a) in a face-centered cubic structure, Zn-rich η(Al, Zn) phase (in Fig. 4a) in a close-packed hexagonal structure, and the spinel structured $MgAl_2O_4$. The composite also contains the compounds $CuZn_4$ and Al_4C_3. Many small peaks manifesting the existence of nano SiC_p were apparent. Ac-

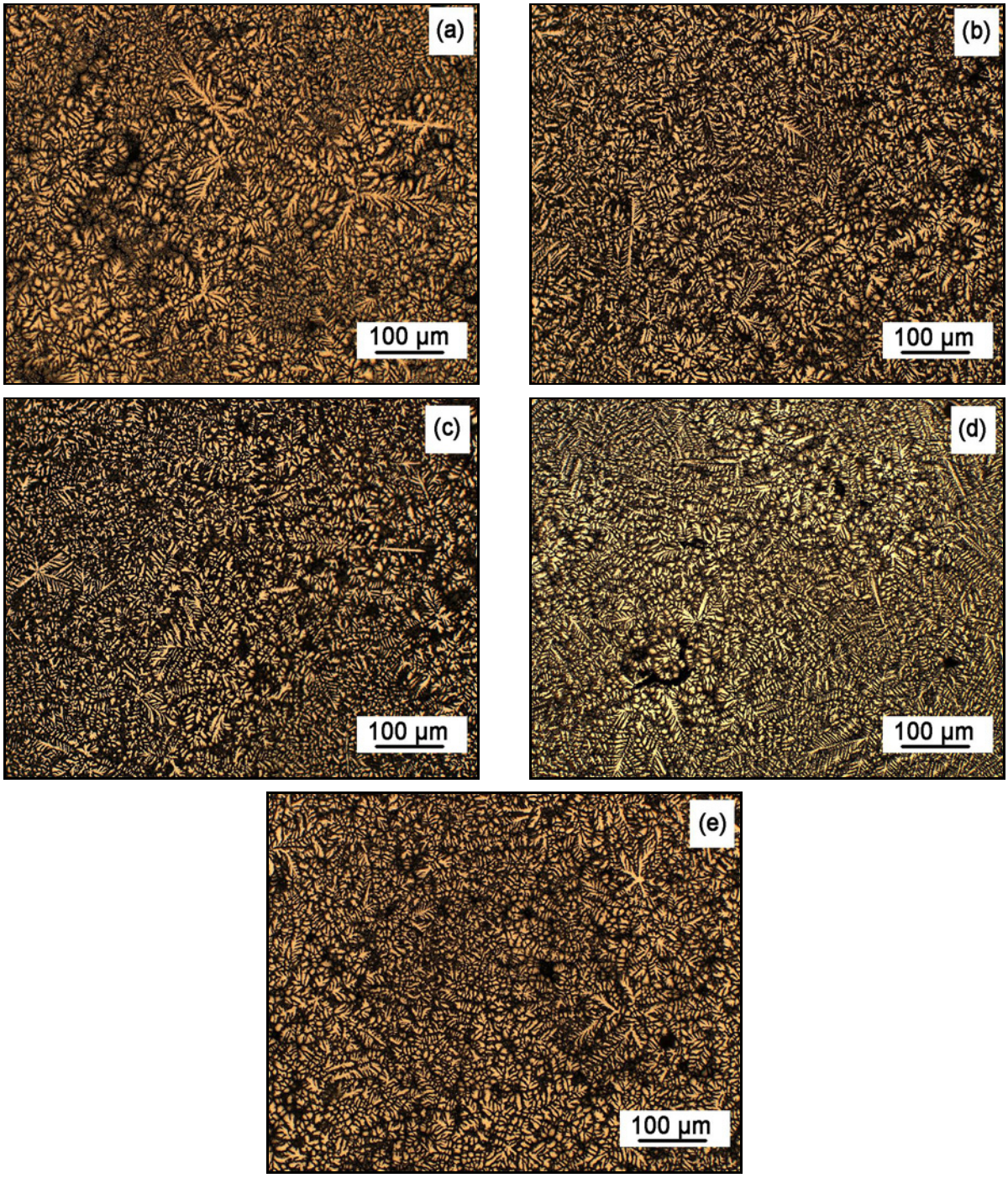

Fig. 3. Five representative as-cast microstructures corresponding to the (a) specimen 2, (b) specimen 6, (c) specimen 7, (d) specimen 10, and (e) specimen 15.

cording to the EDS results, Si was also detected (Spectrum 1) (corresponding to particle marked by red arrow). It is reasonable to conclude that these spherical particles are SiC_p. Most of the SiC_p remain distributed along the grain boundaries of the α and η phases, and a small quantity of SiC_p can be found in the α phase. The appearance of Al_4C_3 indicates an interfacial reaction between the nano SiC_p and the metal matrix.

It was observed that the cooperation of thermal and acoustic fields is essential under the same force field upon comparing and analyzing the data obtained from specimens 2 and 6. When the fusant temperature was high, the effect of ultrasonic vibration was found to be better. The relatively fine and small dendritic crystal will improve the abrasive resistance of the nano-SiC_p/ZA38 composite. Comparison between specimens 2 and 15, under the same acoustic field,

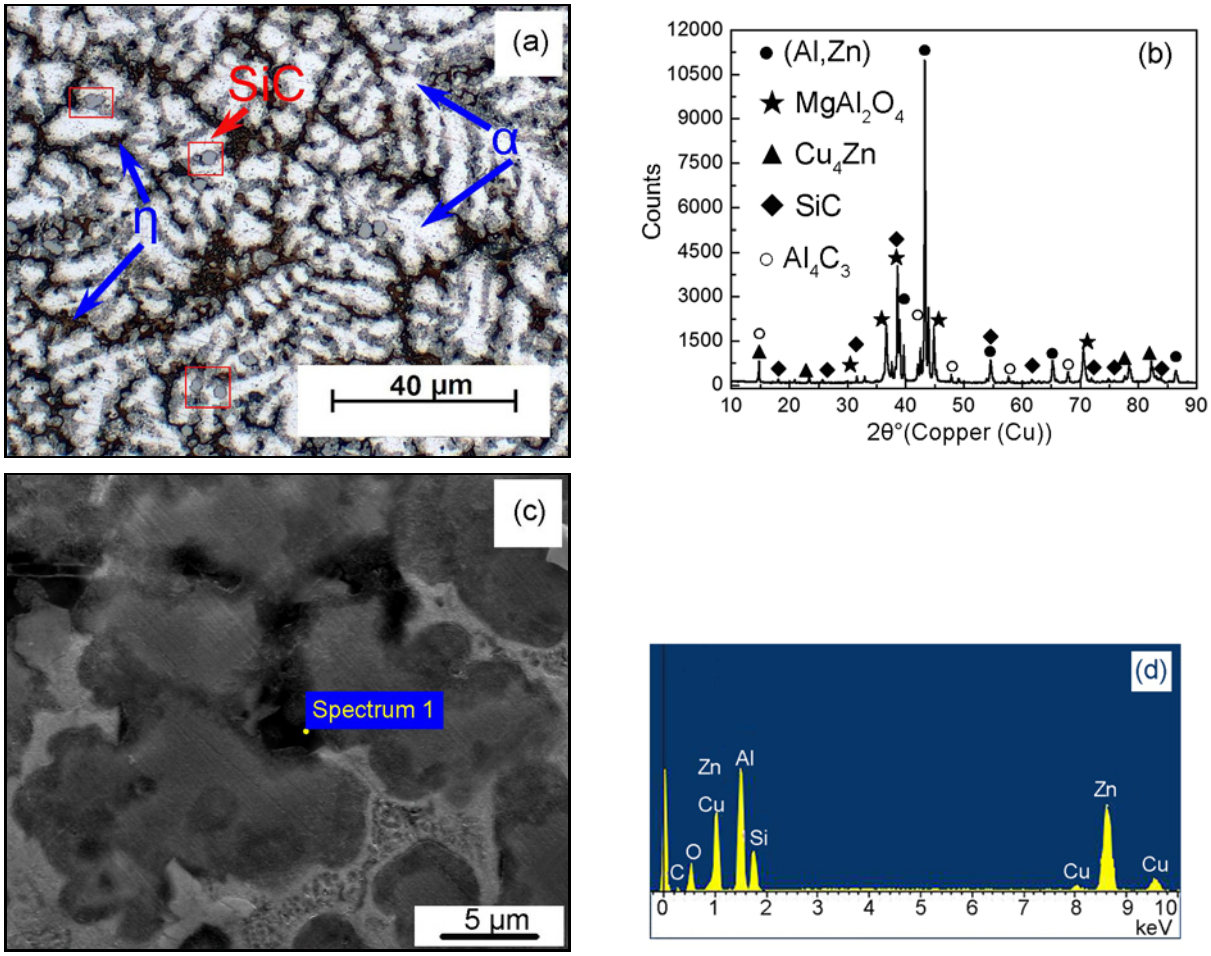

Fig. 4. XRD and EDS analysis to determine the phases in the nano-SiC_p/ZA38 composite: (a) metallographic structure, (b) XRD results, (c) SEM images, and (d) point scanning energy spectrum.

revealed that the increased thermal and force fields could enhance the abrasive resistance of the nano-SiC_p/ZA38 composite. From the microstructures of specimens 2 and 15, it is evident that the dimension of the dendritic crystal α(Al, Zn) phase in specimen 15 is relatively smaller. A comparison between specimens 6 and 7 shows that there is little change in the dimension of the dendritic α(Al, Zn) phase under the same thermal field, while the grain dimension becomes smaller in specimen 7 with the increase in the acoustic and force fields. This results in a better abrasive resistance in specimen 7. In conclusion, a good combination of the technological parameters in the thermal-force-acoustic mixed fields is crucial to obtain the refined microstructure for improving the abrasive resistance of the nano-SiC_p/ZA38 composite.

The corresponding morphologies of friction surfaces are presented in Fig. 5. These indicate an adhesive wear mechanism in the nano-SiC_p/ZA38 composite. Deep plow marks along the friction direction in specimens 2, 6, and 15 are evident. Furthermore, lamellate peeling and overlap friction are quite apparent in specimen 2. The appearance of deep plow marks manifests the extremely unstable frictional state, which results in the decrease of abrasive resistance. The morphologies of specimens 7 and 10 were found to be similar, and the presence of superficial scratches was recorded. This is because the values of micro-hardness of specimens 7 and 10 are both higher than that of other specimens. A higher micro-hardness signifies a lower frictional wear rate (a good abrasive resistance) in the composite. Although the change range in the micro-hardness of specimens is small, a lower micro-hardness will inadvertently accelerate the abrasion.

Figure 6 depicts the compression fracture morphologies of the selected samples. It is observed that the microstructures of specimens 2, 6, and 15 are full of pits, while specimens 7 and 10 have obvious landside sections. The appearance of pits is caused by the aggregation tendency of SiC. Compared to specimen 2, the compression strength increases by 12.4 % in specimen 6 under the same force field. Specimen 6 also shows the presence of an apparent ductile fracture landslide section. In specimen 15, there is a very small change in the compression strength and

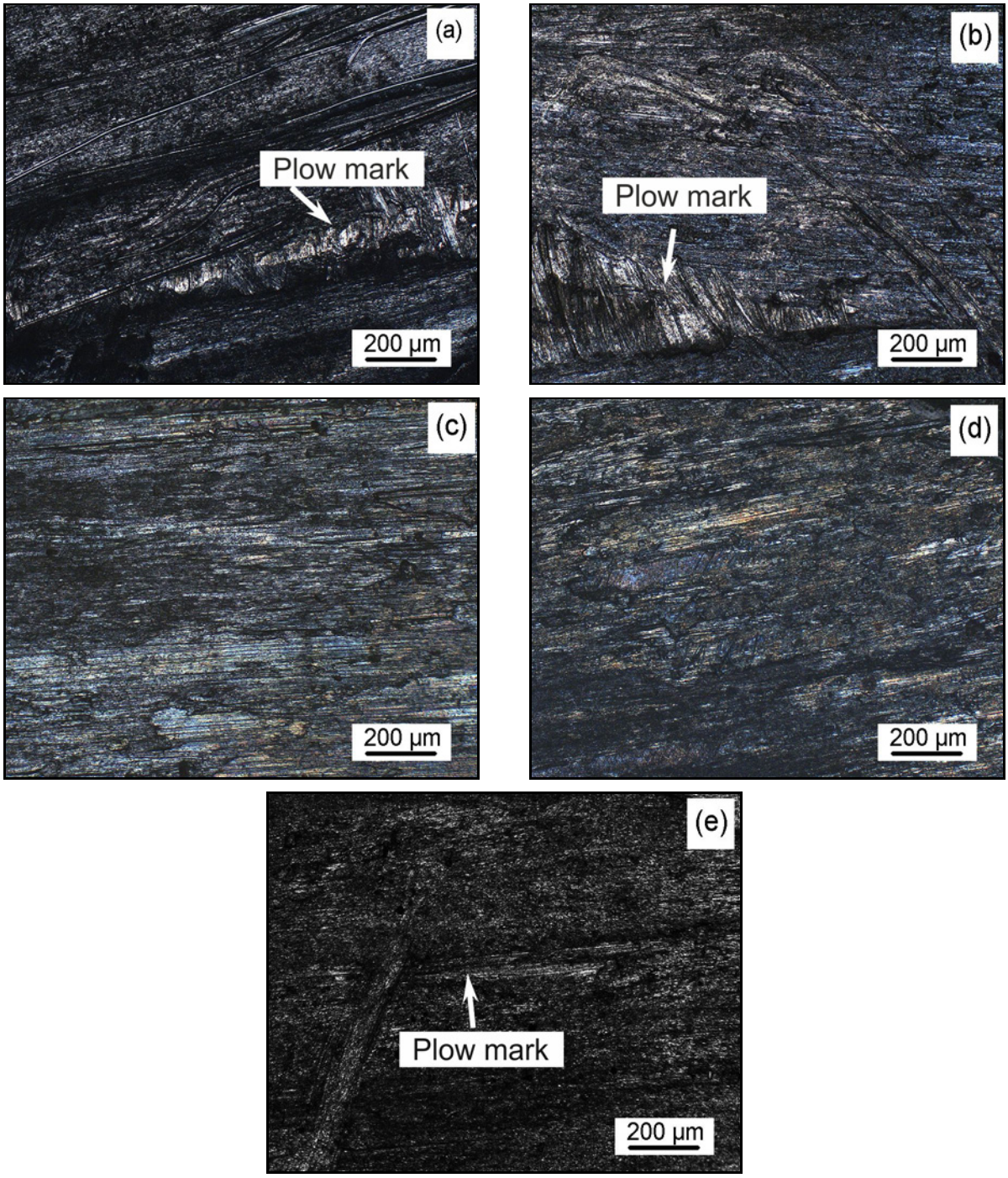

Fig. 5. Morphologies of friction surfaces corresponding to the (a) specimen 2, (b) specimen 6, (c) specimen 7, (d) specimen 10, and (e) specimen 15.

the corresponding fracture morphology compared to specimen 2 under the same acoustic field. Under the same thermal field as in specimen 2, the compression strength increases by 9.1 % in specimen 7, increasing the force and acoustic fields. The increased landside section morphology in specimens 7 and 10 indicates a greater probability of ductile fracture. There are apparent pits manifested by a brittle fracture in cases of the specimen with lower compression strength.

Figure 7 exhibits the relationships between the wear rate and the primary dendrite arm spacing in all the specimens. The different thermal-force-acoustic mixed fields obtained from the particle size distribution calculation software (*Nano measurer 1.2.0.*) were used for the studies. It was observed that the wear rate decreases with the dimension of the arm spacing. The primary dendrite arm spacing in specimen 7, which shows excellent properties, is about 4.81 μm,

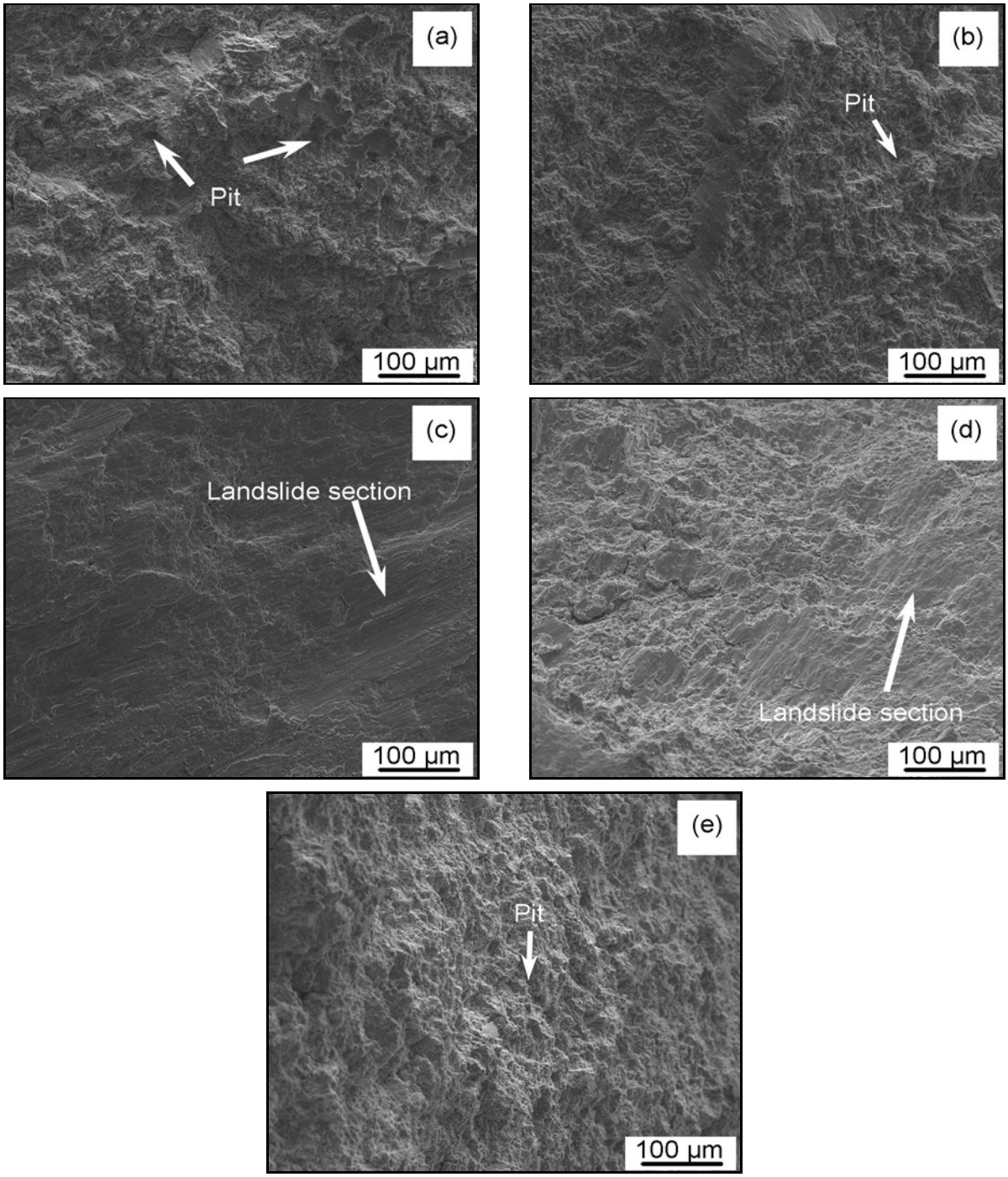

Fig. 6. Fracture morphologies of (a) specimen 2, (b) specimen 6, (c) specimen 7, (d) specimen 10, and (e) specimen 15.

while the arm spacing is about 11.48 μm in specimen 1, which showed the worst wear rate. With an increasing force and acoustic field from specimens 1 to 4 under the same thermal field, the primary dendrite arm spacing decreases. A comparison between specimens 3 to 1 shows that the force and acoustic field increase by three times and two times, respectively. The primary dendrite arm spacing decreases by 51.54 %. However, data from specimens 13 to 16 shows that with an alternate increase in the force and acoustic field, the range of change of the primary dendrite arm spacing dimension is small. It was observed that the wear resistance properties of specimens 1–4 are better than those of specimens 13–16. Moreover, it was concluded that a synchronous or solely higher thermal-force-acoustic field does not ensure better nano-SiC_p/ZA38 composite properties. Therefore, the synergistic effect of the thermal-force-acoustic field should be simultaneously considered.

Specimens 7, 10, and 12 have a relatively smaller

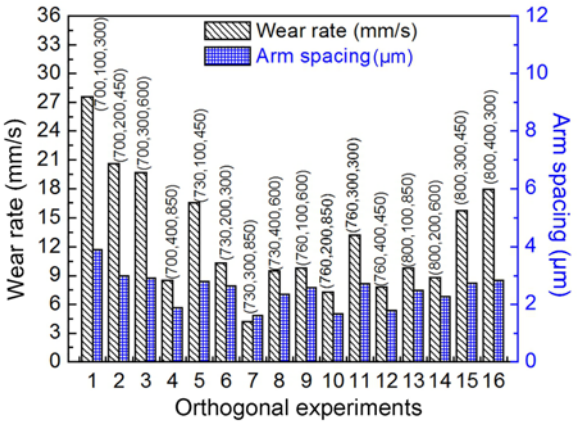

Fig. 7. Relationships between the wear rate and the primary dendrite arm spacing in all specimens.

primary dendrite arm spacing than other specimens. This indicates that the force and acoustic field perform better when the fusant temperature is around 730–760 ℃. Under the same strong acoustic field of specimens 7 and 10, a small change in the thermal and force fields has little effect on the microstructure of the studied composite. The same result can be observed for specimens 10 and 12. The thermal-force-acoustic mixed fields could improve the dispersion of the nano reinforced particles and accelerate the phase change in the metal matrix of the composite. The stirring process increases infiltration behavior and also introduces gas into the fusant. While the ultrasonic transmitter is located below the fusant, the effects of the cavitation and acoustic streaming by the ultrasonic vibration fasten the formation of cavitation bubbles and nucleation, thus leading to grain refinement.

When ultrasonic power increases, the range of acoustic pressure also increases. At the same time, the required critical radius for the cavitation bubbles decreases. The energy released from the explosion of cavitation bubbles will lash and cause the cluster nano reinforced SiC particles to vibrate. This accelerates particle dispersion. A series of changes in the microstructure of the nano-SiC_p/ZA38 composite was reinforced by nano SiC particles under the thermal-force-acoustic mixed fields. When the thermal field is considered, it is observed that heating increases with the increase of the fusant temperature. The proportion of the reinforced particles with the metal matrix increases and thus deteriorates the infiltration of the reinforced particles. Moreover, the higher fusant temperature causes the burning loss of the composite. The nano-reinforced particles can easily immerse in the metal matrix at an increased speed of stirring when the force field is separately considered. However, the dispersibility of the reinforced particles could not be improved. The infiltrating effect of reinforced particles was not optimized when the acoustic field was separately considered. It is better to improve the problems as mentioned above by the coordination of the mixed thermal-force-acoustic fields. Nonetheless, some problems could not be ignored. For instance, the higher thermal field results in a lower viscosity of the composite fusant, increasing its flowability. In this case, the fusant is easy to spatter under a higher force field, and the ultrasound cavitation effect is disturbed. Suppose the thermal field is insufficient, and the force field is low enough. In that case, the infiltrating effect of reinforced particles is not guaranteed, and the retarding effect caused by the ultrasound cavitation is stimulated. In the thermal-force-acoustic mixed fields, the thermal and force field separately determines the fusant viscosity and laminar motion of the composite fusant. The acoustic field influences the crushing degree of the reunion block in the fusant and further changes the fusant crystallization.

Due to the driving force introduced by the force and the acoustic fields under the thermal-force-acoustic mixed fields, the proportions of multiple compositions are balanced. This decreases the amount of critical nucleation during solidification and increases the critical undercooling of the studied composite. The wear-resistant α phase and the antifriction η phase [9] both get refined in specimen 7 (Fig. 3). During the friction of the composite, only the superficial scratches can be observed in specimen 7, while deep plow marks are apparent in specimens 2, 6, and 15. The refined microstructure shows slippery and rough fracture surfaces (Fig. 6), representing the cleavage and quasi-cleavage sections, respectively. This signifies excellent toughness and antifriction capability. Finally, the abrasive resistance of the nano-SiC_p/ZA38 composite could be substantially improved.

In a word, it is concluded that the microstructures of developed nano-SiC_p/ZA38 composite material mainly depend on the synergistic effects of the thermal-force-acoustic field. The three fields have their different effect on the final microstructure and properties. The finer primary dendrite arm and grains will be obtained by multiple combinations among the three fields. It is generally inferred that the effect of the acoustic field increases with the fusant temperature under the same force field. Besides, it is beneficial to refine the microstructure by improving the thermal and force fields under the same acoustic field. Under the same thermal field, the grain size decreases with the increase of acoustic and force fields. Nevertheless, the simultaneously improved three fields could not further refine the microstructure and improve the properties due to the interference between the higher flowability and ultrasound cavitation effect.

4. Conclusions

In the present study, the nano-SiC_p/ZA38 composite material reinforced by nano SiC particles was fabricated by stirring assisted ultrasonic vibration. Orthogonal experiments with four different fusant temperatures, stirring speed, and ultrasonic power were conducted to ascertain the relationship among the fusant temperature, stirring speed, and ultrasonic power on the mechanical and tribological properties of the cast nano-SiC_p/ZA38 composite material.

The major conclusions are:

(1) The wear rate decreases to 0.0042 mm s^{-1}, the minimum value, in the specimen by melting at 730 ℃, at a stirring speed of 300 rpm and ultrasonic treatment with a power of 850 W. The hardness reaches 163.9 HV, and the compression strength reaches 803 MPa.

(2) The acoustic field improves the mechanical properties of the nano-SiC_p/ZA38 composite, while the thermal and acoustic fields play a major role in the friction and wear properties. The force fields turn into an assistant field. A higher thermal-force-acoustic mixed field value does not imply an enhancement in the mechanical properties of the nano-SiC_p/ZA38 composite.

(3) The wear rate decreases with the dimension of the primary dendrite arm spacing.

Acknowledgements

The authors gratefully acknowledge the financial supports from the National Natural Science Foundation of China (NSFC) (52004193), the China Postdoctoral Science Foundation (2020M682496), National Training Programs of Innovation and Entrepreneurship for Undergraduates (202110488004), Guidance Programs of Science and Technology Research for Hubei Provincial Department of Education (B2020008), WUST National Defence Pre-research Foundation (GF202006), the Postdoctoral Innovative Research Post of Hubei Province, and the Post-doctoral Research Funding Program of Jiangsu Province.

References

[1] S. Liu, Q. Yuan, Y. Q. Gong, Y. L. Zhou, L. X. Li, G. Xu, Correlations between microstructure and dry friction wear behavior of Zn-38Al-3.5Cu-1.2 Mg alloy reinforced with SiC nanoparticles, Trans. Indian Inst. Met. 72 (2019) 2557–2565. doi:10.1016/j.jma.2016.09.002

[2] H. Çuvalci, H. Baş, Investigation of the tribological properties of silicon containing zinc-aluminum based journal bearings, Tribol. Int. 37 (2004) 433–440. doi:10.1016/j.triboint.2003.10.006

[3] T. Savaşkan, R. A. Maleki, Friction and wear properties of Zn-25Al-based bearing alloys, Tribol. Trans. 57 (2014) 435–444. doi:10.1080/10402004.2014.880540

[4] B. Bobbi, J. Bajat, I. Bobić, B. Jegdić, Corrosion influence on surface appearance and microstructure of compo cast ZA27/SiC_p composites in sodium chloride solution, T. Nonferr. Metal. Soc. 26 (2016) 1512–1521. doi:10.1016/S1003-6326(16)64257-7

[5] S. Murphy, T. Savaskan, Comparative wear behaviour of Zn-Al-based alloys in an automotive engine application, Wear 98 (1984) 151–161. doi:10.1016/0043-1648(84)90224-2

[6] S. K. Mishra, S. Biswas, A. Satapathy, A study on processing, characterization and erosion wear behavior of silicon carbide particle filled ZA-27 metal matrix composites, Mater. Des. 55 (2014) 958–965. doi:10.1016/j.matdes.2013.10.069

[7] T. Savaşkan, R. A. Maleki, H. O. Tan, Tribological properties of Zn-25Al-3Cu-1Si alloy, Tribol. Int. 81 (2015) 105–111. doi:10.1016/j.triboint.2014.08.014

[8] M. T. Abou El-khair, A. Lotfy, A. Daoud, A. M. El-Sheikh, Microstructure, thermal behavior and mechanical properties of squeeze cast SiC, ZrO_2 or C reinforced ZA27 composites, Mater. Sci. Eng. A 528 (2011) 2353–2362. doi:10.1016/j.msea.2010.11.060

[9] S. Liu, Q. Yuan, Y. Q. Gong, G. Xu, W. W. Qiao, Relationship between microstructure and dry wear behavior of compo-cast nano-$SiC_{(p)}$+ micro-$Gr_{(p)}$/Zn-35Al-1.2Mg-0.2Sr composite under different chilling conditions, Kovove Mater. 50 (2020) 49–57. doi:10.4149/km_2020_1_49

[10] K. B. Nie, X. J. Wang, K. Wu, X. S. Hu, M. Y. Zheng, L. Xu, Microstructure and tensile properties of micro-SiC particles reinforced magnesium matrix composites produced by semisolid stirring assisted ultrasonic vibration, Mater. Sci. Eng. A 528 (2011) 8709–8714. doi:10.1016/j.msea.2011.08.035

[11] Q. Li, F. Qiu, Q. C. Jiang, B. X. Dong, R. Geng, M. M. Lv, Q. L. Zhao, Q. C. Jiang, Fabrication, microstructure refinement and strengthening mechanisms of nanosized SiC_P/Al composites assisted ultrasonic vibration, Mater. Sci. Eng. A 735 (2018) 310–317. doi:10.1016/j.msea.2018.08.060

[12] K. B. Nie, X. J. Wang, K. Wu, L. Xu, M. Y. Zheng, X. S. Hu, Processing, microstructure and mechanical properties of magnesium matrix nanocomposites fabricated by semisolid stirring assisted ultrasonic vibration, J. Alloys Compd. 509 (2011) 8664–8669. doi:10.1016/j.jallcom.2011.06.091

[13] L. Y. Chen, J. Y. Peng, J. Q. Xu, H. Choi, X. C. Li, Achieving uniform distribution and dispersion of a high percentage of nanoparticles in metal matrix nanocomposites by solidification processing, Scripta Mater. 69 (2013) 634–637. doi:10.1016/j.scriptamat.2013.07.016

[14] N. Srivastava, G. P. Chaudhari, Microstructural evolution and mechanical behavior of ultrasonically synthesized Al6061-nano alumina composites, Mater. Sci. Eng. A 724 (2018) 199–207. doi:10.1016/j.msea.2018.03.092

[15] H. Khosravi, H. Bakhshi, E. Salahinejad, Effects of compocasting process parameters on microstructural characteristics and tensile properties of A356-SiC_p composites, T. Nonferr. Metal. Soc. 24 (2014) 2482–2488. doi:10.1016/S1003-6326(14)63374-4

[16] X. J. Wang, N. Z. Wang, L. Y. Wang, X. S. Hu, K. Wu, Y. Q. Wang, Y. D. Huang, Processing, microstructure and mechanical properties of micro-SiC

particles reinforced magnesium matrix composites fabricated by stir casting assisted by ultrasonic treatment processing, Mater. Des. 57 (2014) 638–645. doi:10.1016/j.matdes.2014.01.022

[17] K. Hu, D. Yuan, S. L. Lv, S. S. Wu, Effects of nano-SiC_p content on microstructure and mechanical properties of SiC_p/A356 composites assisted with ultrasonic treatment, T. Nonferr. Metal. Soc. 28 (2018) 2173–2180. doi:10.1016/S1003-6326(18)64862-9

[18] A. H. Idrisi, A. H. I. Mourad, Conventional stir casting versus ultrasonic assisted stir casting process: Mechanical and physical characteristics of AMCs, J. Alloys Compd. 805 (2019) 502–508. doi:10.1016/j.jallcom.2019.07.076

[19] R. Kumar, S. Chauhan, Study on surface roughness measurement for turning of Al 7075/10/SiC_p and Al 7075 hybrid composites by using response surface methodology (RSM) and artificial neural networking (ANN), Measurement 65 (2015) 166–180. doi:10.1016/j.measurement.2015.01.003

[20] M. M. Porter, L. Meraz, A. Calderon, H. Choi, A. Chouhan, L. Wang, M. A. Meyers, J. McKittrick, Torsional properties of helix-reinforced composites fabricated by magnetic freeze casting, Compos. Struct. 119 (2015) 174–184. doi:10.1016/j.compstruct.2014.08.033

[21] I. Balasubramanian, R. Maheswaran, V. Manikandan, N. Patil, M. A. Raja, R. M. Singari, Mechanical characterization and machining of squeeze cast AZ91D/SiC magnesium based metal matrix composites, Procedia Manuf. 20 (2018) 97–105. doi:10.1016/j.promfg.2018.02.014

[22] S. Sardar, S. K. Karmakar, D. Das, High stress abrasive wear characteristics of Al 7075 alloy and 7075/Al_2O_3 composite, Measurement 127 (2018) 42–46. doi:10.1016/j.measurement.2018.05.090

[23] L. Natrayan, M. S. Kumar, Optimization of wear behaviour on AA6061/Al_2O_3/SiC metal matrix composite using squeeze casting technique-statistical analysis, Mater. Today: Proceedings 27 (2020) 306–310. doi:10.1016/j.matpr.2019.11.038

[24] N. Singh, R. Singh, I. P. S. Ahuja, I. Farina, F. Fraternali, Metal matrix composite from recycled materials by using additive manufacturing assisted investment casting, Compos. Struct. 207 (2019) 129–135. doi:10.1016/j.compstruct.2018.09.072

[25] J. Sreejith, S. Ilangovan, Optimization of wear parameters of binary Al-25Zn and Al-3Cu alloys using design of experiments, Int. J. Miner. Metall. Mater. 25 (2018) 1465–1472. doi:10.1007/s12613-018-1701-9

[26] Q. Yuan, G, Xu, M, Liu, H. J. Hu, J. Y. Tian, Effects of rolling temperature on the microstructure and mechanical properties in an ultrafine-grained low-carbon steel, Steel Res. Int. (2018) 90. doi:10.1002/srin.201800318

[27] Q. Yuan, G. Xu, S. Liu, M. Liu, H. J. Hu, G. Q. Li, Effect of rolling reduction on microstructure and property of ultrafine grained low-carbon steel processed by cryorolling martensite, Metals 8 (2018) 518–531. doi:10.3390/met8070518

[28] X. L. Gan, Q. Yuan, G. Zhao, H. J. Hu, J. Y. Tian, G. Xu, Investigating the properties of coil tail in Ti-Nb-Mo microalloyed hot-rolled strip, Steel Res. Int. 90 (2019) 1–9. doi:10.1002/srin.201900040

[29] X. L. Gan, Q. Yuan, G. Zhao, H. W. Ma, W. Liang, Z. L. Xue, W. W. Qiao. G. Xu, Quantitative analysis of microstructures and strength of Nb-Ti microalloyed steel with different Ti additions, Metall. Mater. Trans. A 51 (2020) 2084–2096. doi:10.1007/s11661-020-05700-9

[30] Q. Yuan, G. Xu, M. Liu, S. Liu, H. J. Hu, Evaluation of mechanical properties and microstructures of ultrafine grain low-carbon steel processed by cryorolling and annealing, Trans. Ind. Inst. Met. 72 (2019) 741–749. doi:10.1007/s12666-018-1526-2